complex. The reduction step for the sulfenato complex was not observed, but the sulfinato derivative did react about 160 times more slowly than the parent cysteinato complex. This contrasts markedly with the reduction rate that occurs when an alkyl substituent is placed on sulfur (**12** and **15** in Table X); in these reactions, the substituted derivative is reduced almost 10^5 times slower than the parent thiolato species. It is interesting to note that the coordinated sulfenato system produces the coupled product, cystine, upon reduction, in the same way as is postulated to occur when sulfur radical ions are produced in purely organic systems.[43] There is no evidence in our work that the metal complexes are able to compete with the radical for the dimerization process, even in an intramolecular fashion. Sulfur compounds such as cysteamine and cysteine have been proposed to act as radical repair agents that protect against the effects of ionizing radiation.[44,45] It seems clear from our work that they would also protect the metal centers of proteins from the effects of very reducing radicals since the sulfur radicals would preferentially couple to form dimers rather than pass the electron onto a metal.

Acknowledgment. We are grateful to the Research Corp. for a Cottrell Grant that aided this work in its early stages. We are further indebted to the National Institutes of Health for a grant that allowed for the completion of this study (Grant No. GM31383).

Registry No. **5**, 94110-44-8; **6**, 62698-05-9; Cr, 7440-47-3; $[Cr(OH_2)_5(CysO_2)]^+$, 94136-14-8.

Supplementary Material Available: Full sets of kinetic data for Tables I-III, VI, and VII (8 pages). Ordering information is given on any current masthead page.

(43) Hoffman, M. Z.; Hayon, E. *J. Phys. Chem.* **1973**, *77*, 990.
(44) Adams, G. E.; McNaughton, G. S.; Micheal, B. D. *Trans. Faraday Soc.* **1968**, *64*, 902.
(45) Adams, G. E.; Armstrong, R. C.; Charlesby, A.; Michael, B. D.; Willson, R. L. *Trans. Faraday Soc.* **1969**, *65*, 732.
(46) Oae, S. "Organic Chemsitry of Sulfur"; Oae, S., Ed.; Plenum Press: New York, 1977; pp 406-13.

Contribution No. 6968 from the Arthur Amos Noyes Laboratory, California Institute of Technology, Pasadena, California 91125

Electronic Absorption and Emission Spectra of Dioxorhenium(V) Complexes. Characterization of the Luminescent ^3E_g State

JAY R. WINKLER and HARRY B. GRAY*

Received June 15, 1984

The low-temperature single-crystal-polarized electronic absorption spectra of three *trans*-dioxorhenium(V) ions, $ReO_2L_4^z$ (L = CN^-, $z = 3-$; L = $^1/_2$en, $z = 1+$; L = py, $z = 1+$), have been investigated. The spectra display up to four distinct band systems that exhibit vibrational progressions in a high-energy (750-800-cm^{-1}) mode. The two lowest energy band systems (500-550 nm) are assigned to components of a $^3E_g[b_{2g}(xy)^1e_g(xz,yz)^1 \leftarrow b_{2g}(xy)^2]$ excited state that is split by spin-orbit coupling interactions. The next higher energy band (400-450 nm) is assigned to the corresponding ^1E_g state, whereas the fourth band (ca. 300 nm) must arise from a different one-electron excitation. Luminescence from at least two of the lowest energy ^3E_g components in the cyanide and pyridine complexes has been detected, and the zero-field splitting between the two emitting states is 10-20 cm^{-1}. At 5 K, only the lowest energy component is populated and the luminescence spectra from this state display progressions in a ca. 900-cm^{-1} mode that corresponds to the symmetric rhenium-oxygen stretching vibration. Franck-Condon analyses of the luminescence bands indicate distortions of 0.09 (1) and 0.07 (1) Å along each Re-O bond for the cyanide and pyridine complexes, respectively. The lower energy of the corresponding progressions in absorption and the π-antibonding character of the ^3E_g state suggest that the excited-state distortion is an elongation. The luminescence spectrum of the pyridine complex also exhibits a progression in a 190-cm^{-1} mode indicative of a 0.03 (1) Å distortion along the symmetric Re-py stretching coordinate. The lifetime of the ^3E_g state at room temperature varies from 10 to 300 μs in crystals and is about 10 μs for $ReO_2(py)_4^+$ (and its substituted pyridine analogues) in aprotic solvents. The luminescence of these dioxorhenium species, however, is rather efficiently quenched by protic solvents such as water and alcohols.

Introduction

The importance of oxidation reactions of organic compounds and the capacity of many metal-oxo reagents to effect such transformations have stimulated a great deal of research into the structures and reactivity of these high-valent transition-metal complexes. Stoichiometric oxidation reactions of organic substrates by d^0 oxo complexes of Mn, Cr, Ru, and Os are quite well-known and extensively studied.[1] These reagents are commonly used in organic synthesis, and the mechanisms of their reactions have been examined both experimentally and theoretically.[2] In addition, metal oxides and mixed-metal oxides are currently used in catalytic oxidations, and oxo species are even suspected in biochemical oxygenase reactions.[3,4] Clearly, metal-oxo complexes are exceptionally valuable chemical reagents.

One of the goals of our research on metal-oxo species has been to develop reagents that will photochemically oxidize organic substrates. Since an electronically excited metal-oxo complex is one reagent in a reaction of this sort, we believe it is necessary to examine, in detail, by electronic spectroscopy, its physical and structural properties. We have already communicated our initial results from spectroscopic studies of some luminescent dioxorhenium(V) complexes.[5] In this paper we fully describe the electronic spectra and structures of these complexes as well as their excited-state decay properties in crystals and solutions.

Experimental Section

Procedures. Dichloromethane (Burdick and Jackson) was degassed with five freeze-pump-thaw cycles on a high-vacuum line ($<10^{-3}$ torr) and stored under vacuum over activated (heating under vacuum for 12

(1) (a) Stewart, R. In "Oxidation in Organic Chemistry", Part A; Wiberg, K. B., Ed.; Academic Press: New York, 1962; pp 1-68. (b) Wiberg, K. B. Reference 1a, pp 69-184. (c) Lee, D. G.; van den Engh, M. In "Oxidation in Organic Chemistry"; Part B; Trahanovsky, W. S., Ed.; Academic Press: New York, 1973; pp 177-227. (d) Collin, R. J.; Jones, J.; Griffith, W. P. *J. Chem. Soc., Dalton Trans.* **1974**, 1094-1097.
(2) Rappé, A. K.; Goddard, W. A., III. *J. Am. Chem. Soc.* **1982**, *104*, 3287-3294.
(3) Sheldon, R. A.; Kochi, J. K. *Adv. Catal.* **1976**, *25*, 272-413.
(4) (a) Groves, J. T.; McClucky, G. A. *J. Am. Chem. Soc.* **1976**, *98*, 859-861. (b) Loew, G. H.; Kert, C. J.; Hjelmeland, L. M.; Kirchner, R. F. *Ibid.* **1977**, *99*, 3534-3536. (c) Balch, A. L. *Ibid.* **1980**, *102*, 1446-1448. (d) Loew, G. H.; Herman, Z. S. *Ibid.* **1980**, *107*, 6174-6175. (e) Hanson, L. K.; Chang, C. K.; Davis, M. S.; Fajer, J. *Ibid.* **1981**, *103*, 663-670.
(5) Winkler, J. R.; Gray, H. B. *J. Am. Chem. Soc.* **1983**, *105*, 1373-1374.

0020-1669/85/1324-0346$01.50/0

h) Linde type 4A molecular sieves. Tetrahydrofuran, THF (Burdick and Jackson), was refluxed over and distilled from a mixture of sodium metal and benzophenone under an Ar atmosphere, degassed with five freeze–pump–thaw cycles, and stored under vacuum over sodium and benzophenone. After a few days, the THF solution acquired the characteristic purple color of the benzophenone dianion. Pyridine (Burdick and Jackson) was refluxed under Ar and over sodium metal, distilled, degassed with five freeze–pump–thaw cycles, and stored under vacuum over CaH_2. Spectroscopic grade acetone (Baker) was degassed with five freeze–pump–thaw cycles and stored under vacuum over activated Linde 4A molecular sieves. When needed, these solvents were transferred by flask-to-flask distillation on a high-vacuum line and further degassed with three freeze–pump–thaw cycles. All other solvents were reagent grade unless otherwise specified. Elemental analyses were obtained at the Caltech Analytical Laboratory.

$K_3ReO_2(CN)_4$. This salt was prepared by the method of Beard et al.[6] A final crystallization by slow evaporation of an aqueous solution of $K_3ReO_2(CN)_4$ produced large, well-formed rhombic crystals that were characterized by oscillation and Weissenberg X-ray photographs.[7]

$[ReO_2(py)_4]BPh_4$ (py = Pyridine, Ph = C_6H_5). The iodide salt of this dioxorhenium cation was prepared by the procedure of Beard et al.[8] The tetraphenylborate salt was isolated by addition of an aqueous solution of $NaBPh_4$ to one of $[ReO_2(py)_4]I$. The resulting yellow solid was filtered and washed with water. Large crystals of this species were grown by layering petroleum ether over a 4:1 acetone:pyridine solution containing the complex. As the petroleum ether diffused into the lower layer, large red prismatic crystals of $[ReO_2(py)_4]BPh_4$ formed. Anal. Calcd: C, 61.90; H, 4.72; N, 6.56. Found: C, 61.76; H, 4.79; N, 6.57.

$[ReO_2(py\text{-}d_5)_4]BPh_4$ (py-d_5 = C_5D_5N). This complex was prepared by the same procedure used for the pyridine analogue but replacing H_2O with D_2O (Aldrich; 99.8 atom % D) and pyridine with pyridine-d_5 (Aldrich; 99 atom % D).

$[Re^{18}O_2(py)_4]BPh_4$. Finely ground K_2ReCl_6 (1.02 g), prepared by the published procedure,[9] and $AgBF_4$ (0.438 g) were mixed with 1 mL of $H_2{}^{18}O$ (Merck, Sharp, and Dohme; 97 atom %) under an Ar atmosphere. The solution was degassed with five freeze–pump–thaw cycles, and 5 mL of dry pyridine was then added to the mixture by flask-to-flask distillation on the vacuum line. The mixture was refluxed overnight under a static pressure of Ar to yield a red solution and some Ag nuggets. The solvent was stripped off under vacuum and the residue taken up with absolute ethanol (U.S. Industrial Chemical Co.) and filtered. One equivalent of $NaBPh_4$ was added to the filtrate, the white NaCl filtered, and petroleum ether added to precipitate an orange solid. A layer of petroleum ether was vacuum distilled over a 5:1 dry acetone:pyridine solution containing the complex and allowed to diffuse into the lower layer, producing red crystals. Infrared spectra of the natural-abundance and ^{18}O samples exhibit antisymmetric rhenium–oxygen stretching vibrations at 815 and 780 cm^{-1}, respectively.

$[ReO_2(4\text{-pic})_4]BPh_4$ (4-pic = 4-Picoline). A mixture of K_2ReCl_6 (0.5 g), 4-picoline (ca. 10 mL), and H_2O (ca. 1 mL) was refluxed for 20 h. One equivalent of $NaBPh_4$ was added to the homogeneous solution to precipitate an orange solid that was recrystallized from a mixture of water and 4-picoline. Large crystals were grown by diffusion of petroleum ether into a 4:1 acetone:4-picoline solution containing the complex. Anal. Calcd: C, 63.36; H, 5.32; N, 6.16. Found: C, 63.25; H, 5.36; N, 6.17.

$[ReO_2(4\text{-}t\text{-Bupy})_4]BPh_4$ (4-*t*-Bupy = 4-*tert*-Butylpyridine). A mixture of K_2ReCl_6 (0.5 g), 4-*tert*-butylpyridine (6 mL), and H_2O (ca. 1 mL) was refluxed for 12 h. The solution was heated to boiling to drive off the H_2O and, upon cooling, an orange solid precipitated that was recrystallized from 4-*tert*-butylpyridine and water. The BPh_4^- salt was prepared by mixing $[ReO_2(4\text{-}t\text{-Bupy})_4]Cl$ (95.2 mg) and $NaBPh_4$ (53.25 mg) in a two-phase mixture of 4-*tert*-butylpyridine (5 mL) and water (5 mL) and stirring overnight. The organic layer was then separated, and petroleum ether was added to precipitate an orange solid. Crystals were grown by diffusion of petroleum ether into a 4:1 acetone:4-*tert*-butylpyridine solution containing the complex. Anal. Calcd: C, 66.84; H, 6.73; N, 5.20. Found: C, 66.63; H, 6.75; N, 5.18.

$[ReO_2(en)_2]Cl$ (en = Ethylenediamine). This complex was prepared by the method of Murmann.[10] Large crystals were grown by evaporation of an aqueous solution containing the complex. The salt was characterized by oscillation and Weissenberg X-ray photographs.[11]

Absorption Spectra. Electronic spectra were recorded on a Cary Model 17 spectrophotometer. Low temperatures were achieved with either a CTI Model 21 cryocooler (300–30 K) or an Andonian Associates Model 024 liquid-helium (L-He) Dewar system (77–4.5 K). Temperatures in the cryocooler were measured with a chromel/Au–Fe thermocouple, and the temperature could be varied with a small resistive heater. The temperature at the sample in the L-He Dewar was monitored with a calibrated glassy-carbon resistor mounted in a brass block in thermal contact with the sample. The temperature could be adjusted with a resistive heater that warmed the He gas before it passed over the sample. Polarized spectra were recorded along crystal extinction directions with a pair of Glan–Thompson calcite polarizers. Extinction directions were determined spectrophotometrically by rotating the polarizers to absorption maxima and minima. Single crystals for absorption spectra were mounted on fused silica disks and masked with "copper grease" (a mixture of fine copper powder and Apiezon H grease). Crystal faces were determined by examination under a polarizing microscope and by X-ray photography.

Luminescence Spectra. Luminescence spectra were recorded on an instrument constructed at Caltech and described previously.[12] Both the cryocooler and the Dewar were used for low-temperature measurements. The spectrometer response was determined with a calibrated tungsten filament lamp, and spectra were corrected for this response by the method of Drushel, Sommers, and Cox.[13] Solid samples were single crystals or polycrystalline arrays mounted on fused silica disks with Dow Corning high-vacuum silicone grease. Solution samples were prepared under vacuum in a 10-mL round-bottom flask equipped with a side-arm 1-cm fluorescence cuvette.

Luminescence Lifetimes. Luminescence lifetimes were measured by a Quanta Ray DCR Nd–YAG laser system that has been described elsewhere.[14] Variable-temperature experiments between 300 and 80 K were performed with a glass Dewar through which flowed nitrogen gas that had been cooled by passage through a coil of copper tubing immersed in a Dewar of liquid nitrogen. Temperatures between 80 and 4.5 K were achieved with the Andonian L-He Dewar. In both Dewars, emitted light was collected off the front (excited) surface of the sample. The laser flash lamp energy was generally set just above threshold for solid samples, because higher laser powers typically led to nonexponential decays. Solution samples were prepared in a cell identical with that used for luminescence spectra.

Luminescence Quantum Yields. Absolute luminescence quantum yields were determined by the method of Demas and Crosby.[15] Solutions were rigorously degassed with no fewer than five freeze–pump–thaw cycles. The absorbances of these solutions were less than 0.1 (1 cm) at the 436-nm excitation wavelength. The quantum yield standard was $[Ru(2,2'\text{-bpy})_3]Cl_2$ (Sigma Chemical Co.) in water (NANOpure, vide infra), which has a reported quantum yield of 0.042 with 436-nm excitation.[16]

Stern–Volmer Quenching. Investigations of bimolecular photochemical reactivity were performed by the Stern–Volmer quenching method.[17] Luminescence quenching was monitored by steady-state or time-resolved luminescence measurements. These two techniques yield equivalent results only if no static quenching (i.e., ground-state complex formation between emitter and quencher) mechanism is active. Lifetime measurements, therefore, provide a more direct probe of excited-state reactivity and were generally chosen over their steady-state counterparts. Samples were prepared in a vessel similar to that used for solution luminescence experiments but which was connected to the vacuum line via a U-tube in which samples could be degassed with freeze–pump–thaw cycles in the case of liquid quenchers or under dynamic vacuum in the case of solids. Once degassed, liquid quenchers were distilled into the 10-mL round-bottom flask, and solids were rinsed into the flask with solvent distilled from the sample solution. Solid quenchers were measured by weight, and a 20-μL Hamilton syringe was used to deliver aliquots of liquid quenchers. All lifetimes were measured with 532-nm excitation.

Quenchers. The following chemicals were used in luminescence quenching experiments. House deionized water was passed through a Barnstead NANOpure water purifying system. Methanol (Burdick and Jackson) was refluxed over sodium metal and distilled. Methanol tended

(6) Beard, J. H.; Calhoun, C.; Casey, J.; Murmann, R. K. *J. Am. Chem. Soc.* **1968**, *90*, 3389–3394.
(7) Murmann, R. K.; Schlemper, E. O. *Inorg. Chem.* **1971**, *10*, 2352–2354.
(8) Beard, J. H.; Casey, J.; Murmann, R. K. *Inorg. Chem.* **1965**, *4*, 797–803.
(9) Hurd, L. C.; Reinders, V. A. *Inorg. Synth.* **1939**, *1*, 178–180.
(10) Murmann, R. K. *Inorg. Synth.* **1976**, *8*, 173–174.
(11) Sergienko, V. S.; Porai-Koshits, M. A.; Khodashova, T. S. *Zh. Strukt. Khim.* **1974**, *15*, 275–281.
(12) Rice, S. F.; Gray, H. B. *J. Am. Chem. Soc.* **1983**, *105*, 4571–4575.
(13) Drushel, H. V.; Sommers, A. L.; Cox, R. C. *Anal. Chem.* **1963**, *35*, 2166–2172.
(14) Nocera, D. G.; Winkler, J. R.; Yocom, K. M.; Bordignon, E.; Gray, H. B. *J. Am. Chem. Soc.* **1984**, *106*, 5145–5150.
(15) Demas, J. N.; Crosby, G. A. *J. Phys. Chem.* **1971**, *75*, 991–1024.
(16) vanHouten, J.; Watts, R. J. *J. Am. Chem. Soc.* **1976**, *98*, 4853–4858.
(17) Balzani, V.; Moggi, L.; Manfrin, M. F.; Bolleta, F. *Coord. Chem. Rev.* **1975**, *15*, 321–433.

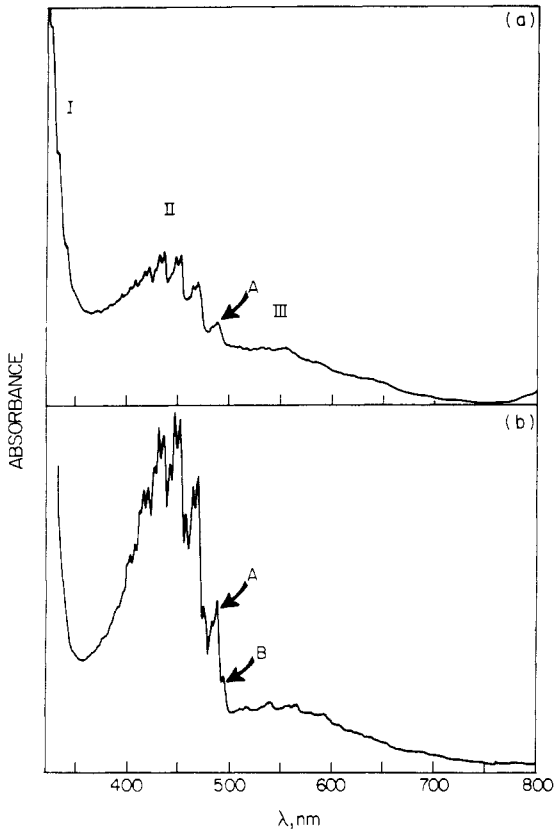

Figure 1. Single-crystal-polarized electronic absorption spectra of $[ReO_2(en)_2]Cl$ at 30 K: (a) perpendicular orientation of the electric field of the incident light and the crystal needle axis; (b) parallel orientation of the electric field and needle axis.

to break round-bottom flasks when thawed so, rather than freezing in liquid nitrogen, the solvent was degassed by repeatedly cooling in a dry ice/acetone slurry, evacuating, and warming to room temperature. Similarly, methanol was transferred under vacuum by flask-to-flask distillation by cooling the receiving flask in a dry ice/acetone bath. Absolute ethanol (U.S. Industrial Chemical Co.), D_2O (Aldrich; 99.8+ atom % D), CH_3OD (Aldrich; 99.5+ atom % D), C_2H_5OD (Aldrich; 99.5+ atom % D), and CD_3OD (Aldrich; 99.5+ atom % D) were all used without further purification. All of these quenchers, except water, were stored under a static pressure of Ar gas during a quenching experiment and were transferred against an Ar flow. Pyridinium tetraphenylborate, $(pyH)(BPh_4)$, was prepared by addition of an aqueous solution of $NaBPh_4$ to a mixture of 5 mL of pyridine and 5 mL of concentrated HCl. The white solid that precipitated was filtered, washed with water, and air-dried. The compound was recrystallized from an acetone/light petroleum ether mixture.

Results

Spectroscopy. The room-temperature electronic absorption spectra of the three dioxorhenium ions, $ReO_2(en)_2^+$, $ReO_2(py)_4^+$, and $ReO_2(CN)_4^{3-}$, are very similar at wavelengths longer than 400 nm, being characterized by one band maximizing between 400 and 450 nm with a less intense shoulder on the low-energy side. The 400-nm band is relatively weak in the cyanide and ethylenediamine complexes ($\epsilon < 50$ M^{-1} cm^{-1}) but is considerably more intense in the pyridine complex ($\epsilon \sim 1200$ M^{-1} cm^{-1}). A great deal more information about the electronic structures of these dioxorhenium ions is provided by their low-temperature absorption spectra and the luminescence spectra and lifetimes of the cyanide and pyridine complexes.

The 30 K polarized electronic absorption spectra of a $[ReO_2(en)_2]Cl$ crystal are reproduced in Figure 1. The monoclinic crystals[11] of this complex grow as needles, the axis of which is roughly parallel to the crystallographic *a* axis. The spectrum recorded with the electric field vector of the incident light oriented perpendicular to the needle axis is given in Figure 1a, whereas Figure 1b corresponds to the parallel orientation of the electric field and the needle axis. Three distinct absorption systems appear

Table I. Vibronic Peak Maxima and Spacings of Band II in the 30 K Absorption Spectrum of $[ReO_2(en)_2]Cl$ (Perpendicular Polarization)

band	λ_{max},[a] nm	$\tilde{\nu}$, cm^{-1}	energy sep, cm^{-1}	
A	489.9	20 412		
			241	
	484.2	20 653		824
	470.9	21 236	228	
	465.9	21 464		
	460.8	21 701	237	810
	453.6	22 046	231	
	448.9	22 277		
	444.3	22 507	230	801
	437.7	22 847	226	
	433.4	23 073		
	429.2	23 299	226	799
	422.9	23 646	232	
	418.8	23 878		
	414.8	24 108	230	798
	409.1	24 444	229	
	405.3	24 673		
	401.5	24 907	234	

[a] Uncertainties are ±0.2 nm.

in these spectra (labeled I, II, and III), although band I is too intense to be resolved in the parallel polarization. Band I maximizes at a wavelength shorter than 320 nm and progresses in a ca. 800-cm^{-1} mode. Band II, which corresponds to a 440-nm absorption maximum at room temperature, is much less intense than band I and, in the perpendicular polarization, displays progressions in modes of 800 and 225 cm^{-1}. Peak maxima and separations are listed in Table I. In the parallel polarization, a new set of peaks appears in band II, the lowest energy component of which is labeled B. These peaks lie approximately 220 cm^{-1} to the red of the first components of the 225-cm^{-1} progression found in the perpendicular polarization (the lowest energy member is labeled A), but their different polarizations demonstrate that they do not, in fact, belong to this progression. Peaks A and B, therefore, probably correspond to vibronic origins for band II. Although band II is less intense in the perpendicular polarization on this crystal face, it is not so on other crystal faces (corresponding to rotations about the needle axis), and the spectrum of $[ReO_2(en)_2]Cl$ in a KCl disk at 30 K more closely resembles Figure 1a. The progressions built on vibronic origin B are, therefore, much less intense than those built on A. Finally, the low-energy shoulder in the room-temperature spectrum resolves into band III at 30 K, which exhibits an 800-cm^{-1} progression. Band III, however, is very complex and extends from 500 to beyond 650 nm. Significantly, no luminescence was detected from the $ReO_2(en)_2^+$ ion in either the solid state or aqueous solution.

The single-crystal-polarized electronic absorption spectra of $[ReO_2(py)_4]BPh_4$ at 30 K are shown in Figure 2. The crystals grow as prismatic needles, and the spectrum in Figure 2a corresponds to the parallel orientation of the needle axis and the electric field vector of the incident light, whereas Figure 2b represents the perpendicular orientation. The 420-nm absorption maximum in the room-temperature spectrum of this ion is too intense to be observed at low temperature in a crystal, but the low-energy shoulder resolves into a discrete, highly structured absorption profile (band III) with a maximum near 500 nm. Band III in the parallel polarization is composed of a 780-cm^{-1} vibrational progression subdivided by vibronic maxima with 160–180-cm^{-1} separations. The more closely spaced peaks do not, however, correspond to a ca. 170 cm^{-1} progression, because they exhibit disparate polarization behavior and their relative intensities are not commensurate with a harmonic Franck–Condon progression.[18] In addition, two very small features that comprise band system IV appear at 590.1 (2) and 597.1 (2) nm, but they have neither the proper energy spacings nor intensities to be components of the progressions in band III. Peak maxima and

(18) Ballhausen, C. J. "Molecular Electronic Structures of Transition Metal Complexes"; McGraw-Hill: New York, 1979.

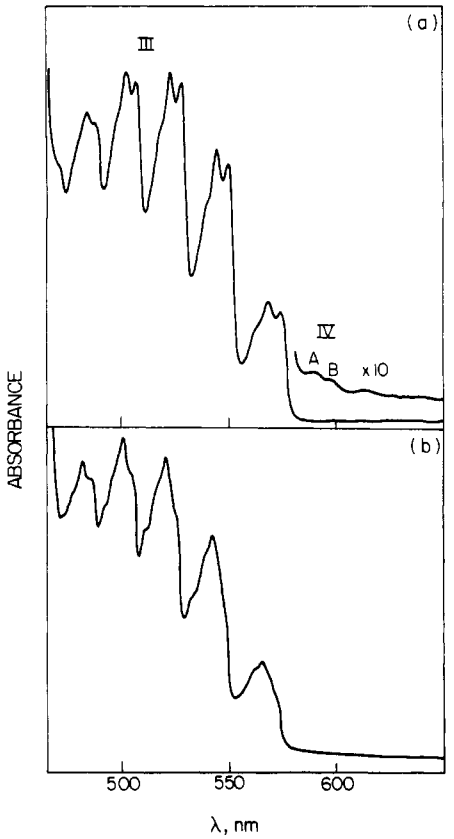

Figure 2. Single-crystal-polarized electronic absorption spectra of $[ReO_2(py)_4]BPh_4$ at 30 K: (a) parallel orientation of electric field and crystal needle axis; (b) perpendicular orientation of electric field and crystal needle axis.

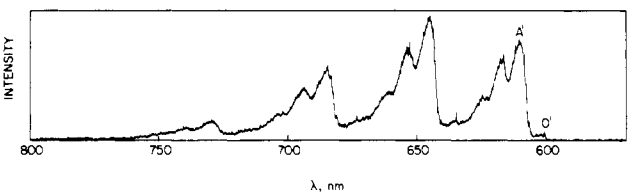

Figure 3. Luminescence spectrum of crystalline $[ReO_2(py)_4]BPh_4$ at 5 K (436-nm excitation) (not corrected for spectrometer response).

energy spacings for bands III and IV are listed in Table II.

Further insight into the $[ReO_2(py)_4]BPh_4$ electronic structure is provided by its low-temperature luminescence spectrum (Figure 3). In contrast to the absorption spectrum, the 4.5 K emission spectrum is particularly straightforward, consisting of two (one 900- and one 190-cm^{-1}) vibrational progressions (peak positions are listed in Table II). The highest energy *real* feature that can be discerned in the 4.5 K luminescence spectrum of this complex is a shoulder (O) at 16 678 (10) cm^{-1} (599.6 (2) nm) on the high-energy edge of peak O′ (Figure 3). Comparison with the origin region of the absorption spectrum (inset, Figure 2a) suggests that O is the electronic origin for the emission band and for part of absorption system IV. This assignment derives primarily from the symmetrical disposition of O, 269 (10) cm^{-1} from peak A in absorption and 268 (10) cm^{-1} from A′ in emission. The peaks A and A′ then correspond to vibronic origins built on the pure electronic origin O. When the sample is warmed to 30 K, the emission spectrum of $[ReO_2(py)_4]BPh_4$ changes dramatically (Figure 4). A new set of peaks resolves, the highest energy component of which is a peak at 16 628 (10) cm^{-1} (B′). This feature is analogous to peak B in the absorption spectrum. The fact that B′ appears only at elevated temperature implies that it corresponds to a state that becomes thermally accessible upon warming from 5 to 30 K. Peaks B and B′ are then vibronic origins of this higher energy state. The position of the electronic origin of this second state can be estimated by assuming that the vibronic

Table II. Vibronic Peak Maxima and Energy Spacings in the 30 K Absorption Spectrum (Parallel Polarization) and 5 K Luminescence Spectrum of $[ReO_2(py)_4]BPh_4$

band	λ_{max},[a] nm	$\tilde{\nu}$, cm^{-1}	energy sep, cm^{-1}	
		Absorption		
IV B	597.1	16 748		
A	590.1	16 946		
	573.9	17 425	174	
	568.2	17 599		
	562.4	17 781	182	783
	549.2	18 208		
	543.9	18 386	178	
	539.0	18 553	167	778
III	526.7	18 986		
	521.8	19 164	178	
	517.3	19 331	167	781
	505.9	19 767		
	501.3	19 948	181	
	497.3	20 109	161	775
	486.8	20 542		
	483.0	20 704	162	
		Emission		
A	609.4	16 410	192	
	616.6	16 218		
	623.8	16 031	187	907
	645.0	15 503		
	652.8	15 318	185	
	661.0	15 129	189	897
	684.6	14 606		
	693.6	14 417	189	
	703.0	14 225	192	937
	731.6	13 669		
	739.7	13 519	150	

[a] Uncertainties are ±0.2 nm.

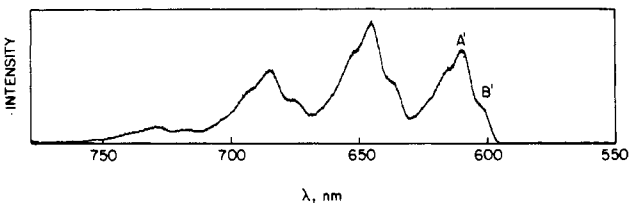

Figure 4. Luminescence spectrum of crystalline $[ReO_2(py)_4]BPh_4$ at 30 K (436-nm excitation) (not corrected for spectrometer response).

promoting mode that gives rise to B and B′ has the same energy in the ground and excited states. The origin of the second state, then, should lie halfway between B and B′, near 16 688 cm^{-1}, or approximately 10 cm^{-1} higher in energy than O. This energy separation is certainly consistent with a state that can be populated at 30 K. The assignment of peaks A and B in the absorption spectrum of $[ReO_2(py)_4]BPh_4$ to vibronic origins of the two luminescent states confirms that band III must correspond to yet another electronic state with an origin near 17 200 cm^{-1} (~581 nm) or about 500 cm^{-1} above O.

Unlike its emission spectrum, the luminescence lifetime of $[ReO_2(py)_4]BPh_4$ does not significantly vary between 5 and 30 K. At 5 K the emission lifetime of crystalline $[ReO_2(py)_4]BPh_4$ is 68 (3) μs and remains so until about 70 K, whereupon it gradually decreases to its room-temperature value of 32 (3) μs. If the analysis of the absorption and emission spectra in terms of two closely spaced (ca. 10 cm^{-1}) electronic states is correct, then the temperature independence of the luminescence decay rate below 70 K implies that the two emitting states have nearly identical decay rates.

The electronic absorption spectra of the isotopically substituted derivatives $[Re^{18}O_2(py)_4]BPh_4$ and $[ReO_2(py\text{-}d_5)_4]BPh_4$ are qualitatively similar to those of their natural-abundance analogues. The 780- and 900-cm^{-1} progressions in absorption and emission, however, reduce to 740 and 850 cm^{-1}, respectively, in the ^{18}O complex. This reduction in frequency by a factor of 0.95 (1) upon ^{18}O substitution is consistent with a symmetric O–Re–O stretching

Table III. Luminescence Lifetimes and Quantum Yields of Dioxorhenium Complexes

complex	solvent	τ,[a] μs	ϕ_{em}[b]
$K_3ReO_2(CN)_4$	crystal	330 (10)	
$[ReO_2(py)_4]BPh_4$	crystal	32 (3)	
	pyridine	17 (2)	0.03 (1)
	THF	13 (2)	0.03 (1)
	CH_2Cl_2	4 (1)	
$[ReO_2(py\text{-}d_5)_4]BPh_4$	crystal	140 (5)	
	THF	9 (2)	0.04 (1)
$[Re^{18}O_2(py)_4]BPh_4$	crystal	36 (3)	
	pyridine	15 (2)	0.03 (1)
$[ReO_2(4\text{-pic})_4]BPh_4$	crystal	11 (2)	
	THF	17 (2)	0.02 (1)
$[ReO_2(4\text{-}t\text{-Bupy})_4]BPh_4$	crystal	11 (2)	
	THF	21 (2)	0.03 (1)

[a] Measured with 532-nm excitation and 650-nm detection (ambient temperature). [b] Measured with 436-nm excitation (ambient temperature).

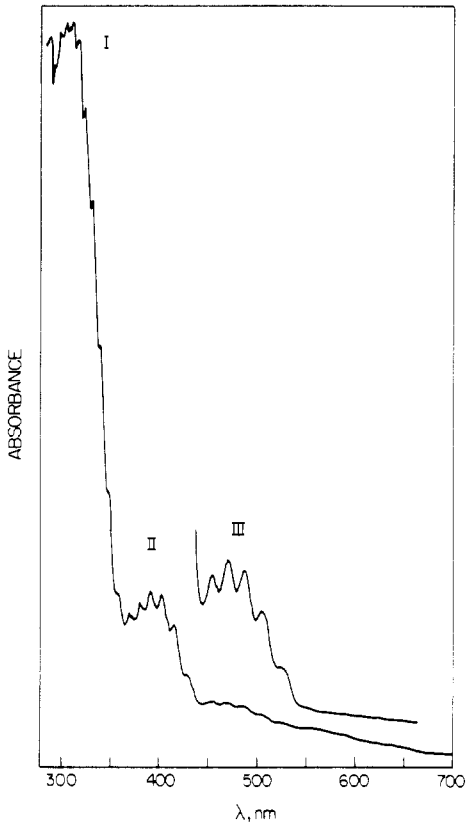

Figure 5. Single-crystal electronic absorption spectrum of $K_3ReO_2(CN)_4$ at 5 K.

vibration where the theoretical reduction factor is 0.94. The vibronic features in the pyridine-d_5 complex spectra are sharper and slightly blue shifted relative to their counterparts in the ^1H complex. The lifetimes of crystalline samples of these as well as two para alkyl substituted pyridine species are listed in Table III. Deuteration of the pyridine rings lengthens the excited-state lifetime by about a factor of 4, para alkyl substitution reduces it by about a factor of 3, and ^{18}O substitution has very little effect.

The low-temperature electronic absorption spectrum of a single crystal of $K_3ReO_2(CN)_4$ is particularly complex (Figure 5). The spectrum is further complicated by the fact that $K_3ReO_2(CN)_4$ crystallizes in the triclinic space group $P\bar{1}$,[7] which permits the crystal extinction directions to rotate as a function of the wavelength of the incident light.[19] Polarization studies, therefore, become very difficult indeed, and few conclusions will be formed

(19) Born, M.; Wolf, E. "Principles of Optics", 2nd ed.; Pergamon Press: New York, 1964.

Table IV. Vibronic Peak Maxima and Spacings in the 30 K Absorption Spectrum and 5 K Luminescence Spectrum of $K_3ReO_2(CN)_4$

band	λ_{max},[a] nm	$\tilde{\nu}$, cm^{-1}	energy sep, cm^{-1}
	Absorption		
	529.9	18 871	
	522.4	19 142	768
	509.2	19 639	
	502.5	19 900	
	494.4	20 227	765
	490.1	20 404	
	484.0	20 661	
	476.2	21 000	773
	472.2	21 177	
	466.8	21 422	
	459.4	21 768	767
	455.7	21 944	
	454.6	22 997	
	450.9	22 178	763
	443.8	22 533	
	440.4	22 707	
	439.2	22 769	
	435.8	22 946	
	Emission		
A′	570.1	17 541	
B′	571.4	17 501	
D′	574.7	17 400	872
E′	577.1	17 328	
	599.9	16 669	
	601.5	16 625	
	604.8	16 534	869
	607.7	16 455	
	632.9	15 800	
	634.5	15 760	
	638.7	15 657	857
	641.5	15 588	
	669.2	14 943	
	670.9	14 905	
	675.7	14 799	
	679.2	14 723	

[a] Uncertainties are ±0.2 nm.

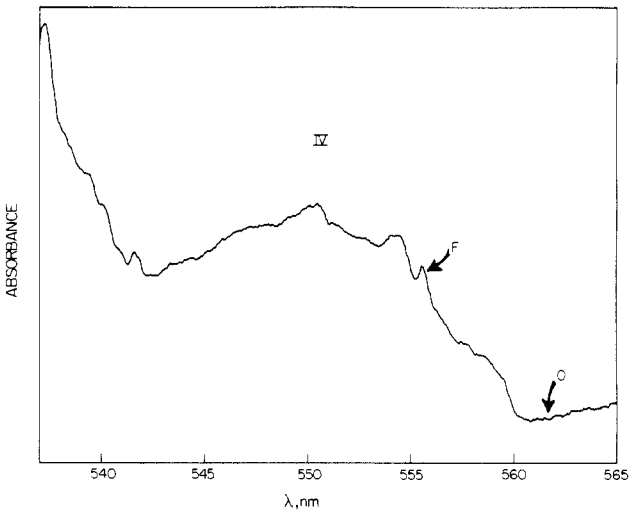

Figure 6. Origin region of the single-crystal electronic absorption spectrum of $K_3ReO_2(CN)_4$ at 30 K.

on the basis of the polarization of these absorption bands. Figure 5 clearly shows three separate absorption bands (I–III) progressing in a high-energy (ca. 770-cm^{-1}) mode and maximizing near 310, 400, and 470 nm. These spectra are actually more highly structured than indicated in Figure 5, and a better resolved spectrum in the region of band III, for example, reveals several sharp absorption features, the positions of which are summarized in Table IV. The origin region of band III (540–560 nm) is shown in Figure 6. The separation and relative intensity of the feature labeled IV demonstrate that it is not a member of the 770-cm^{-1}

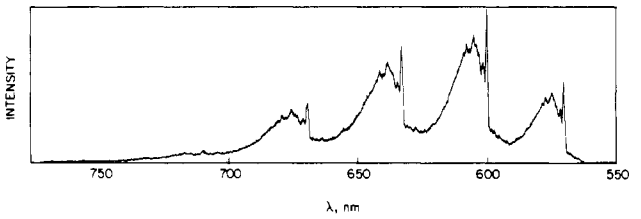

Figure 7. Luminescence spectrum of crystalline $K_3ReO_2(CN)_4$ at 5 K (436-nm excitation) (not corrected for spectrometer response).

Table V. Comparison between Emission Vibronic Maxima and Peaks in the Infrared Spectrum of $K_3ReO_2(CN)_4$ [a]

peak	$\tilde{\nu}$, cm^{-1}	energy from O, cm^{-1}	IR, cm^{-1}
A′	17 541	262 (10)	255
B′	17 501	302 (10)	300 sh
C′	17 461	342 (10)	339
D′	17 400	403 (10)	411
E′	17 328	475 (10)	469, 475

[a] IR spectrum recorded in a Vaseline mull between CsI plates.

progression that comprises band III. The absorption spectrum of $K_3ReO_2(CN)_4$, therefore, exhibits four distinct band systems between 300 and 560 nm, three of which progress in a ca. 770-cm^{-1} mode but none of which displays any lower energy progressions.

The luminescence spectrum of $K_3ReO_2(CN)_4$ at 5 K (Figure 7) is not a great deal simpler than its absorption spectrum. An obvious progression of 870 cm^{-1} resolves at 5 K, but within each member of this progression the spectrum is congested with a number of irregularly spaced and structured emission features (Table IV). A further complication to this spectrum arises upon warming the crystal to 10 K, where several new and distinct emission features appear. It is essentially impossible to understand all of the complex features in these spectra, but it is equally impossible to ignore the few very sharp and prominent features in the luminescence spectrum and their similarity to features in absorption.

The origin regions of these spectra prove to be most enlightening. The highest energy feature in the 5 K emission spectrum of $K_3ReO_2(CN)_4$ (Figure 8) is at 17 803 (10) cm^{-1} (561.7 (2) nm, peak O). No corresponding feature can be detected at this wavelength in the absorption spectrum. If peak O is indeed the electron origin for the 5 K emission band, then the sharp features labeled A′–E′ in Figure 8 are probably vibronic origins built on O. The energy spacings between these peaks and O correlate very well with a number of features in the infrared spectrum of $K_3ReO_2(CN)_4$ (Table V). Another test of the origin assignment for peak O is found in the absorption spectrum and the requirement of mirror symmetry about this origin. Peak O clearly does not fare well in this examination, because no counterparts of peaks A′–E′ are apparent in Figure 6. An escape from this trap is provided by the assumption of heavy spectral congestion in the 550–560-nm absorption region.

The temperature dependence of the luminescence decay rate, in fact, tends to support this assumption. The variation in the luminescence decay rate, k, with temperature is illustrated in Figure 9. This decay rate increases by about a factor of 2 between 5 and 20 K, and, as noted above, new sharp features appear in the emission spectrum at 10 K that are not present at 5 K. These data strongly suggest that, as in the pyridine complex, a second electronic state that can be thermally populated between 5 and 20 K lies just above the lowest energy electronic excited state of $K_3ReO_2(CN)_4$. Additionally, the luminescence intensity increases by about a factor of 1.5 between 5 and 10 K, indicating that the change in k is partly a change in the pure radiative decay rate, which implies a greater oscillator strength for the second state. The absorption spectrum, then, should exhibit mirror symmetry with the higher temperature (10–20 K) emission spectrum. Below 555 nm, the spectra are somewhat symmetric and the origin of the second state lies near 17 816 cm^{-1} (561.3 nm) or about 13 cm^{-1} above peak O.[20] The low-temperature lifetime data also support

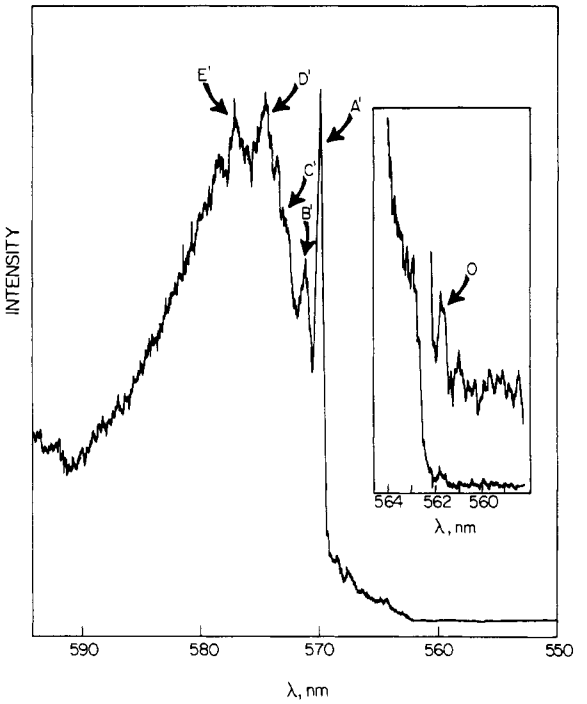

Figure 8. Origin region of the luminescence spectrum of $K_3ReO_2(CN)_4$ at 5 K (436-nm excitation) (not corrected for spectrometer response).

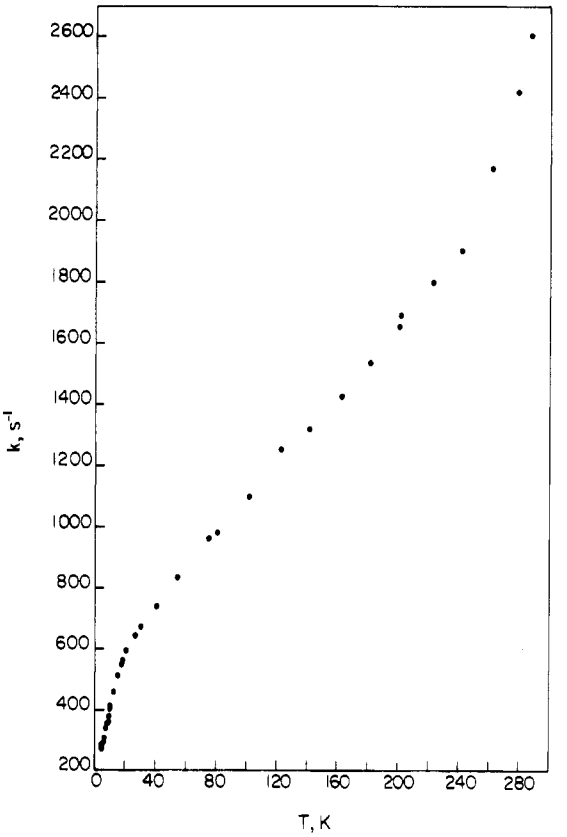

Figure 9. Variation in the luminescence decay rate of $K_3ReO_2(CN)_4$ as a function of temperature between 5 and 300 K.

this conclusion. The luminescence decay rate in the temperature region of 5–50 K is fit well by an expression of the form[21]

$$k_{obsd} = \frac{k_1 + k_2 \exp(-\Delta E/k_B T)}{1 + \exp(-\Delta E/k_B T)} \quad (1)$$

(20) This determination was based on a peak F′ at 17 632 cm^{-1} (567.2 (2) nm) in the 10 K emission spectrum of $K_3ReO_2(CN)_4$ that was assumed to be a vibronic origin, analogous to peak F in Figure 6.

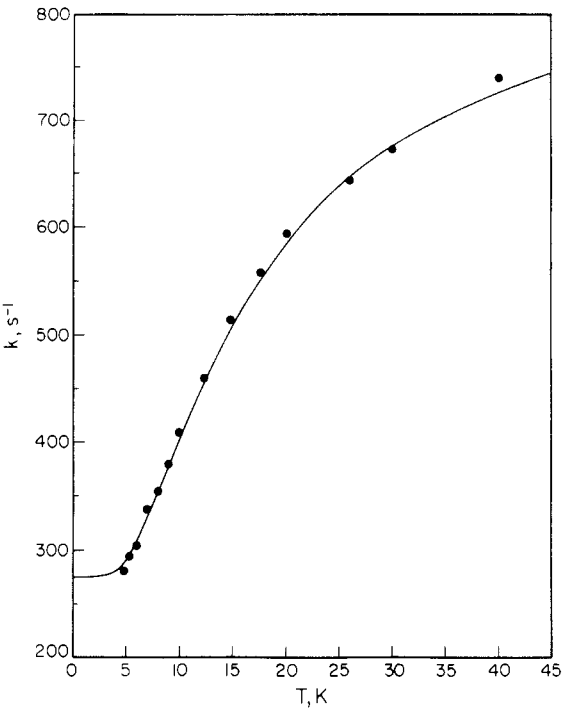

Figure 10. Fit of the variation in luminescence decay rate of $K_3ReO_2(CN)_4$ to eq 1 in the 5–50 K temperature range.

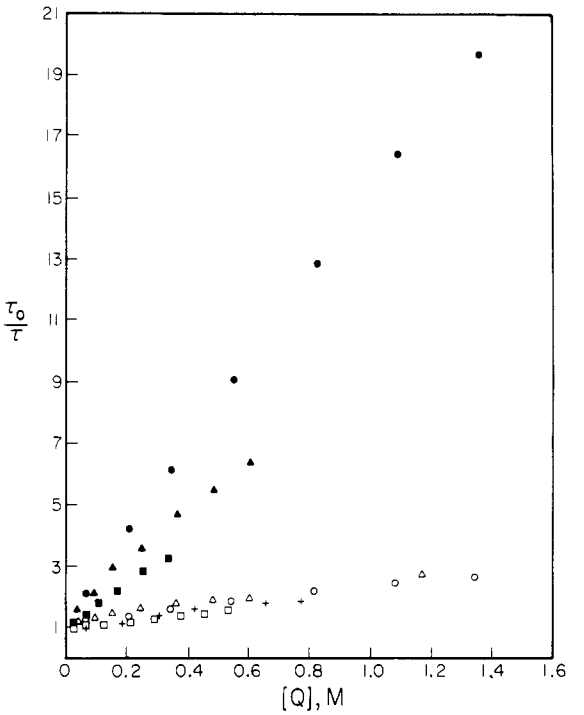

Figure 11. Stern–Volmer plots of the quenching of excited $ReO_2(py)_4^+$ in pyridine: (●) H_2O; (▲) CH_3OH; (■) C_2H_5OH; (○) D_2O; (△) CH_3OD; (+) CD_3OD; (□) C_2H_5OD.

with $k_1 = 275\ s^{-1}$, $k_2 = 1{,}500\ s^{-1}$, and $\Delta E = 15\ cm^{-1}$ (Figure 10). Equation 1 just expresses the observed decay rate for two states in thermal equilibrium that are separated by an energy gap ΔE and have intrinsic decay rates k_1 and k_2. The agreement between ΔE determined from eq 1 and that from the electronic spectra is encouraging. The symmetry between absorption and emission is lost at wavelengths shorter than 555 nm, and it is likely that interference from the origin of band III is responsible. It is also possible that the state or states giving rise to band III cause the further increase in luminescence decay rate above 50 K. The origin of band III probably lies about 400 cm^{-1} above peak O.

The final picture that emerges from the spectra of these dioxorhenium ions is not as complex as the individual spectra suggest. Four discrete band systems can be observed in absorption, three of which exhibit progressions in a high-energy (750–800-cm^{-1}) mode. Band IV, which does not clearly show a high-energy progressions because of interference from the more intense band III, could only be detected in the spectra of the cyanide and pyridine complexes and arises from two very closely spaced (<-20-cm^{-1}) electronic states. The origin of band III lies 400–500 cm^{-1} above the two origins in band system IV but, as with bands I and II, it is not possible to determine the number of electronic states contributing to this absorption feature. Both components of band IV luminesce in the pyridine and cyanide complexes, but no emission was detected from the ethylenediamine species.

Solution Luminescence Properties. The luminescence properties of dioxorhenium ions in solution will be closely related to their photochemical reactivity, because photochemistry is simply a nonradiative decay pathway for an electronically excited molecule. The decay of dioxorhenium excited states is, in fact, quite sensitive to the nature of the solvent. $K_3ReO_2(CN)_4$, for example, is soluble only in water and, as with $ReO_2(py)_4^+$, does not luminesce in this solvent. The tetraphenylborate salt of $ReO_2(py)_4^+$, however, is soluble in aprotic solvents such as CH_2Cl_2, THF, and pyridine, and luminescence from the cation is easily detected in these media. The emission lifetime and quantum yield data for this ion and its isotopically and chemically substituted derivatives are summarized in Table III. The quantum yields, measured with 436-nm excitation, are all in the range of 0.02–0.04, and the excited-state lifetimes vary from 10 to 20 μs. The slight variation in the excited-state lifetime of $[ReO_2(py)_4]BPh_4$ among the solvents pyridine, CH_2Cl_2, and THF is due to subtle medium effects or may simply be a reflection of trace amounts of water in these solvents. The reduction of the $[ReO_2(py\text{-}d_5)_4]BPh_4$ excited-state lifetime in solution relative to its solid-state value, however, is quite significant and suggests that some new lifetime-limiting process is active in solution.

The effect of protic solvents on the luminescence of dioxorhenium ions was investigated by quenching $ReO_2(py)_4^+$ emission in pyridine with the proton donors water, methanol, ethanol, and their deuterated analogues. The ratio of the luminescence lifetime in the absence of quencher to that in the presence of quencher, τ_0/τ, varied linearly with quencher concentration (Figure 11), in agreement with the Stern–Volmer equation.[17] The large deuterium isotope effect demonstrates that the quenching mechanism depends critically upon the hydroxyl protons of these molecules. It is tempting to suggest that simple proton transfer is the deactivation pathway for the luminescent dioxorhenium excited states, but three pieces of evidence suggest otherwise. First, a solution of $[ReO_2(py)_4]BPh_4$ (0.5 mM) in 4 mL of pyridine, 40 μL of CH_3OH (0.25 M), and 170 μL of CH_3OD (~1.0 M) produces a nonexponentially decaying dioxorhenium excited state. The decays, however, are quite nicely fit by single exponentials when either CH_3OH or CH_3OD is used alone as a quencher. Second, addition of these proton donors, especially water, significantly changes the shapes and positions of the emission and absorption bands. Equal amounts of H_2O and D_2O produce roughly comparable changes in band shape. Finally, the relatively strong proton donor pyH^+ ($pK_a = 5.25$)[22] is not an efficient quencher of $ReO_2(py)_4^+$ luminescence even though its pK_a is almost 10 units lower than that of the other proton donors. Clearly, a rather complex mechanism involving both ground and excited states leads to the rapid deactivation of the dioxorhenium excited state in the presence of proton donors.

Discussion

Spectroscopy and Electronic Structure. The electronic spectra and structures of the dioxorhenium ions are probably best ex-

(21) Fordyce, W. A.; Rau, H.; Stone, M. L.; Crosby, G. A. *Chem. Phys. Lett.* **1981**, *77*, 405–408.

(22) "Handbook of Chemistry and Physics", 58th ed.; CRC Press: Cleveland, OH, 1977; p D-127.

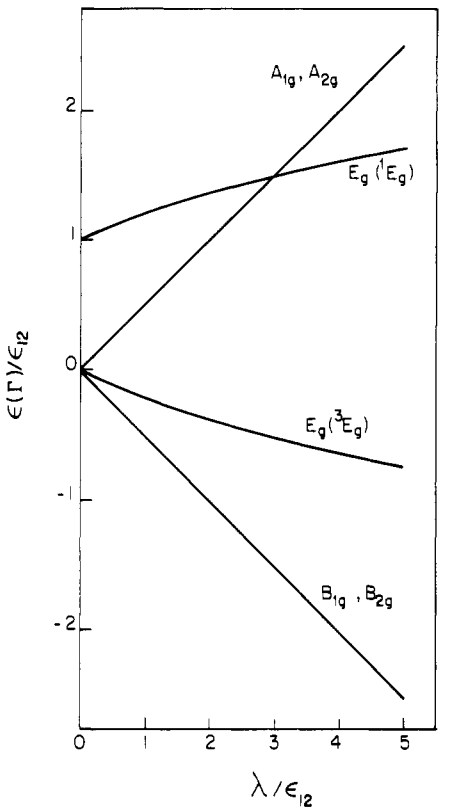

Figure 12. Perturbations of the ^1E_g and ^3E_g states as a result of spin–orbit coupling. ϵ_{12} is the singlet–triplet energy gap in the absence of a spin–orbit coupling perturbation, $\epsilon(\Gamma)$ is the energy of state Γ, and λ is the effective molecular spin–orbit coupling constant.

plained by the following molecular orbital diagram (the reference coordinate system is one in which the Re–O bond coincides with the z axis and the equatorial ligands lie along x and y axes):[23,24]

— $a_{1g}(z^2)$

— $b_{1g}(x^2 - y^2)$

= $e_g(xz, yz)$

— $b_{2g}(xy)$

The dioxorhenium ions possess d^2 metal centers, resulting in a diamagnetic $^1A_{1g}[(b_{2g})^2]$ ground state. The lowest energy ligand field transition involves the promotion of an electron from the $b_{2g}(xy)$ orbital to the doubly degenerate $e_g(xz,yz)$ level, producing $^3E_g[(b_{2g})^1(e_g)^1]$ and $^1E_g[(b_{2g})^1(e_g)^1]$ excited states. Transitions to both excited states are Laporte forbidden ($g \nleftrightarrow g$) and must acquire intensity by vibronic and, in the case of the triplet, spin–orbit coupling mechanisms. The singlet ← singlet transition is likely to be more intense than that to the triplet, and assignments of bands II and III to the $^1E_g[(b_{2g})^1(e_g)^1] \leftarrow {}^1A_{1g}[(b_{2g})^2]$ and $^3E_g[(b_{2g})^1(e_g)^1] \leftarrow {}^1A_{1g}[(b_{2g})^2]$ transitions, respectively, are most appealing. These simple assignments, however, do not account for the two states in band system IV, but their presence can be explained by ligand field theoretical arguments.

A ^3E_g state in D_{4h} symmetry is sixfold degenerate, which in the presence of a strong spin–orbit coupling perturbation will decompose into states of A_{1g}, A_{2g}, B_{1g}, B_{2g}, and E_g symmetries in the D_{4h}' double group, whereas the doubly degenerate ^1E_g state just correlates with an E_g level. A simple first-order spin–orbit coupling calculation produces the diagram in Figure 12.[25] At this level of approximation, the (B_{1g},B_{2g}) and (A_{1g},A_{2g}) pairs are not split by spin–orbit coupling and only the $E_g(^3E_g)$ level can acquire singlet character by mixing with the $E_g(^1E_g)$ state. The abscissa in Figure 12 corresponds to the dimensionless parameter λ/ϵ_{12}, the effective molecular spin–orbit coupling constant divided by the magnitude of the singlet–triplet energy gap in the absence of a spin–orbit coupling perturbation, and the ordinate is just the energy of the state Γ divided by ϵ_{12}. In the limit of large spin–orbit coupling, then, the $(b_{2g})^1(e_g)^1 \leftarrow (b_{2g})^2$ one-electron transition should give rise to at least four absorption bands. Two of these bands, those involving transitions to the E_g states, should be more intense than the other two by virtue of their greater singlet character.

The data are in rather good agreement with the model depicted in Figure 12. The two states that comprise band system IV are most likely the $B_{1g}(^3E_g)$ and $B_{2g}(^3E_g)$ levels. The fact that these are Laporte-forbidden transitions explains the presence in the spectra of vibronic origins built on vanishingly small electronic origins. In both the cyanide and pyridine complexes the zero-field splitting of these two states is less than 20 cm^{-1}, as expected from the ligand field calculation. It is not possible, on the basis of the available data, to determine the relative positions of the B_{1g} and B_{2g} states. Band system III arises from the $E_g(^3E_g) \leftarrow A_{1g}(^1A_{1g})$ transition, accounting for both its greater energy and intensity compared to that of band IV. Band III obscures not only the higher energy region of band IV but probably also the $A_{1g}(^3E_g)$ and $A_{2g}(^3E_g)$ states. The position and intensity of band II argue strongly for its assignment to the $E_g(^1E_g) \leftarrow A_{1g}(^1A_{1g})$ excitation. That bands II and III in the pyridine complex are much more intense than the analogous features in the spectra of the cyanide and ethylenediamine complexes is probably the result of the proximity of charge-transfer states in the pyridine species from which the $E_g(^1E_g)$ and $E_g(^3E_g)$ states could steal intensity. The two complexes, $ReO_2(CN)_4^{3-}$ and $ReO_2(py)_4^+$, fit on the diagram in Figure 12 at λ/ϵ_{12} values of 0.2 and 0.3, respectively. The calculated values of ϵ_{12} and λ are 3900 and 900 cm^{-1}, respectively, for $K_3ReO_2(CN)_4$ and 3900 and 1200 cm^{-1} for $[ReO_2(py)_4]BPh_4$.[26] Finally, band I observed in the cyanide and ethylenediamine complex spectra must arise from a different one-electron transition, perhaps either $a_{1g}(z^2) \leftarrow b_{2g}(xy)$ or oxygen LMCT. In support of this conclusion is the fact that the maximum of band I in $K_3ReO_2(CN)_4$ corresponds to the excitation of more 770-cm^{-1} quanta than in bands II and III.

The low-temperature spectra of these dioxorhenium complexes are rich in vibrational fine structure. All of the bands observed, both in absorption and emission, progress in a high-energy mode that corresponds to the symmetric rhenium–oxygen stretching vibration. Confirmation of this assignment is provided by the spectra of $[Re^{18}O_2(py)_4]BPh_4$ in which the frequency of the progressing mode is 95 (1)% of its value in the natural-abundance complex. That the mode is symmetric is implied by its absence from the infrared spectra of these molecules. These progressions in the rhenium–oxygen stretching vibration indicate a displacement of the potential surfaces of states with the $[e_g(xz,yz)^1b_{2g}(xy)^1]$ configuration relative to that of the $[b_{2g}(xy)^2]$ state. This displacement along the symmetric Re–O coordinate is probably an elongation in the excited state, because the force constant for this vibration is reduced to three-fourths of its ground-state value. Furthermore, a transition that removes an electron from the $b_{2g}(xy)$ orbital and places it in a Re–O π-antibonding $e_g(xz,yz)$ level should result in lengthened metal–oxygen bonds. The magnitude of this distortion can be estimated from the Franck–Condon fits to the 5 K emission spectra of $K_3ReO_2(CN)_4$ and $[ReO_2(py)_4]BPh_4$ (Figures 13 and 14, respectively). Estimated

(23) This ordering of d orbitals in $ReO_2L_4^z$ is predicted on the basis of a similar order in d^1 monooxometal complexes.[24]
(24) Winkler, J. R.; Gray, H. B. *Comments Inorg. Chem.* **1981**, *1*, 257–263.
(25) The details of this calculation are available as supplementary material.
(26) Since only the (B_{1g},B_{2g}), $E_g(^3E_g)$, and $E_g(^1E_g)$ states were located in the spectra, the expressions for the energy separations among these states are symmetric with respect to exchange of λ and ϵ_{12}. Hence, the magnitudes of these parameters are not uniquely determined, and ϵ_{12} was assigned to the larger value. The resulting spin–orbit coupling constants ($\lambda \sim 1000$ cm^{-1}) might seem somewhat small for a high-valent, third-row metal center (Re^V, $\lambda = 3700$ cm^{-1} for the free ion[27]). Quenching of spin–orbit coupling through the intervention of covalency and the Ham effect, however, probably accounts for the discrepancy.[18]
(27) Figgis, B. H. "Introduction to Ligand Fields"; Interscience: New York, 1966; p 60.

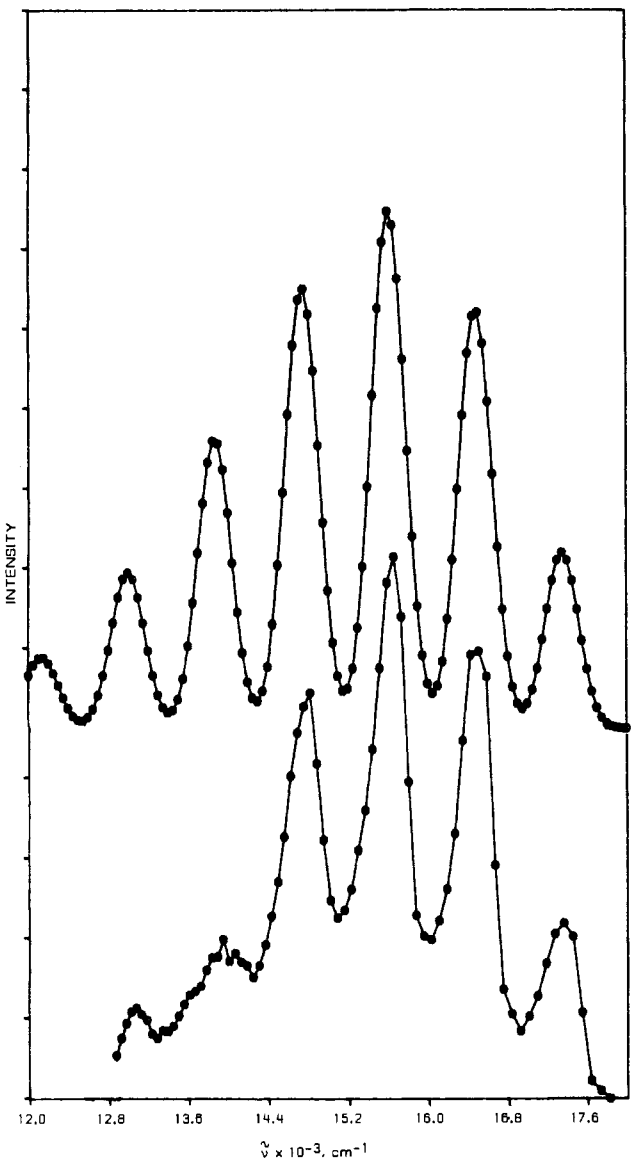

Figure 13. Franck–Condon fit to the 5 K emission spectrum of $K_3ReO_2(CN)_4$ (low resolution): upper spectrum, calculated; lower spectrum, experimental.

distortions of individual Re–O bonds of 0.09 (1) Å for $K_3ReO_2(CN)_4$ (from 1.781 (3) Å in the ground state[7]) and 0.07 (1) Å for $[ReO_2(py)_4]BPh_4$ (from an average ground-state value of 1.76 (1) Å in the chloride salt[28]) were used to generate the calculated spectra in these figures.[29] The emission spectrum of $[ReO_2(py)_4]BPh_4$ displays a second progression (ca. 190-cm^{-1} mode). Hints of an analogous progression are found in band III in the absorption spectrum of this complex. This vibration probably corresponds to the symmetric rhenium–pyridine stretch,[31] and the distortion along this coordinate arises because an electron in a rhenium–pyridine π-bonding orbital, $b_{2g}(xy)$, is involved in the transition. The magnitude of the distortion is calculated to be 0.03 (1) Å (probably an elongation from the average ground-state value of 2.15 (1) Å[28]). The remaining sharp vibronic maxima in the dioxorhenium absorption and emission spectra are either vibronic origins or components of the rhenium–oxygen progressions built on these vibronic origins.

The luminescence decay properties of the $ReO_2(CN)_4^{3-}$ ion prove to be of considerable value in the determination of the

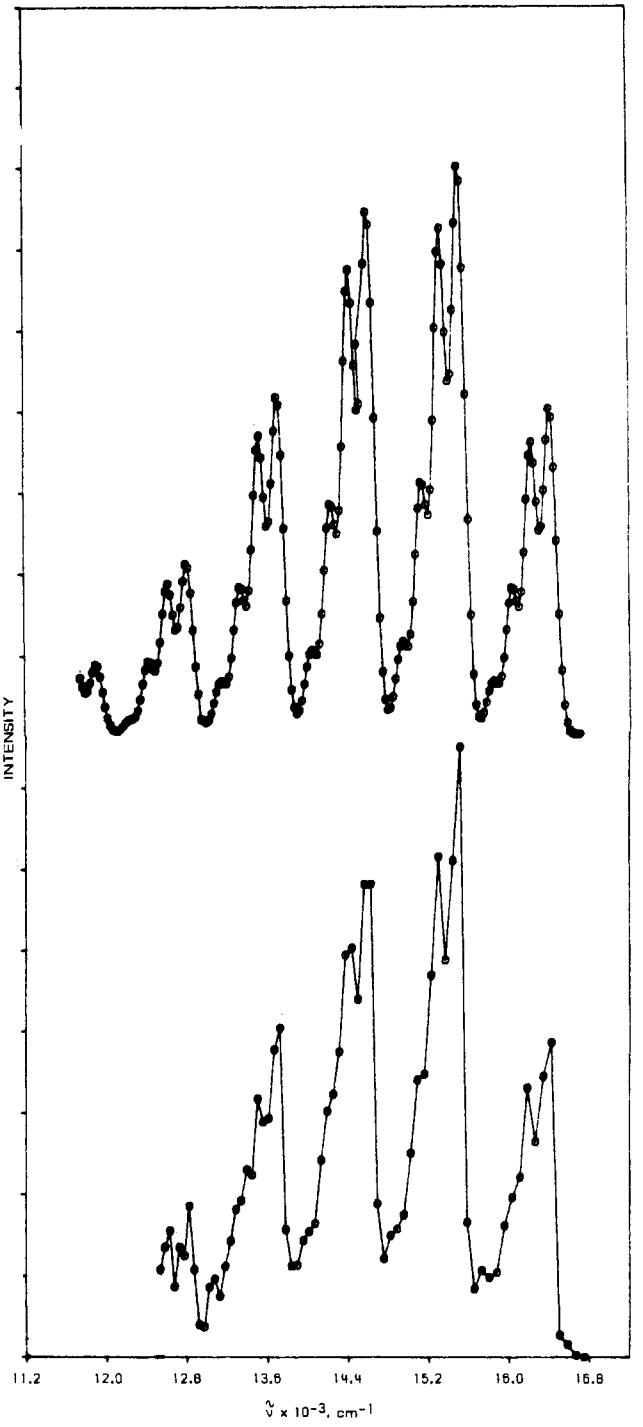

Figure 14. Franck–Condon fit to the 5 K emission spectrum of $[ReO_2(py)_4]BPh_4$: upper spectrum, calculated; lower spectrum, experimental.

electronic structure of this complex. The change in luminescence lifetime as a function of temperature in the 5–20 K region clearly demonstrates the presence of two emitting states. The luminescence lifetimes of both $K_3ReO_2(CN)_4$ and $[ReO_2(py)_4]BPh_4$ decrease by about a factor of 2 upon warming from 70 to 300 K. This temperature dependence could be the result of thermal population of another excited state, presumably $E_g(^3E_g)$ or the intrinsic temperature dependences of the decay rates of the $B_{1g}(^3E_g)$ and $B_{2g}(^3E_g)$ states or both. It is difficult, therefore, to arrive at any meaningful conclusions about the mechanisms of nonradiative decay in these complexes solely on the basis of the temperature dependence of the emission lifetime. One important observation that pertains to nonradiative decay in these complexes is the fact that the excited-state lifetime of crystalline $[ReO_2(py)_4]BPh_4$ increases by about a factor of 4 upon deuteration of the pyridine rings. Similar behavior has been observed upon

(28) Colin, J. L. L.; Turner, G. *Acta Crystallogr., Sect. B: Struct. Crystallogr. Cryst. Chem.* **1978**, *B34*, 923–927.
(29) The details of these calculations are available in ref 30.
(30) Winkler, J. R. Ph.D. Thesis, California Institute of Technology, 1984.
(31) Clark, R. J. H.; Williams, C. S. *Inorg. Chem.* **1965**, *4*, 350–357.

deuteration of the ligands in some Rh(III) pyridyl species.[32] Oxygen-18 substitution, however, does not significantly affect the luminescence lifetime of the $ReO_2(py)_4^+$ cation. This behavior, in which the excited-state decay rate is sensitive to the highest energy vibrational modes in the molecule, exemplifies the weak coupling limit of nonradiative decay theory.[33] In this limit, the relative displacements of ground- and excited-state potential energy surfaces are small and the nonradiative decay rate should exhibit an exponential dependence on the ratio of the energy gap for the transition, ΔE, to the energy of the highest frequency vibrational modes in the molecule, $\hbar\omega_M$.[33] It is clear, then, how perdeuteration of the pyridine rings in $[ReO_2(py)_4]BPh_4$ will increase the lifetime of the dioxorhenium excited states.

The fact that $[ReO_2(en)_2]Cl$ does not luminesce is quite perplexing. The absorption spectrum of this complex is quite similar to those of the pyridine and cyanide analogues, so it is unlikely that major differences is electronic structure account for its radically different nonradiative decay properties. It is possible that the enhanced nonradiative decay in $ReO_2(en)_2^+$ is simply the result of a greater distortion along the high-energy N–H vibrational coordinate that would make them much better accepting modes for the electronic energy than are the less distorted C–H vibrations in the $ReO_2(py)_4^+$ complex.

Solution Luminescence Properties. In order to participate directly and efficiently in bimolecular chemical reactions, the excited dioxorhenium species must live for greater than ca. 50 ns in solution. A very common constituent of many solvents, ionizable hydrogen atoms (i.e., protons), however, very effectively quench these excited metal complexes. The mechanism of quenching by protons is not altogether clear, and though Stern–Volmer kinetics are obeyed with individual quenchers, it is not a simple bimolecular photochemical reaction. Were it so, the binary mixture of CH_3OH and CH_3OD would have yielded an apparent quenching rate constant equal to the sum of the two pseudo-first-order rate constants for the two quenchers. To the contrary, the CH_3OH/CH_3OD mixture produced nonexponential luminescence decay, indicative of two discrete luminescing species that are not in chemical equilibrium with one another. This result, coupled with the fact that the presence of these protic quenchers perturbs both the absorption and emission spectra of $ReO_2(py)_4^+$, argues for some type of complex formation (perhaps via hydrogen bonding) between the dioxorhenium ion and the proton donors. The isotope effect observed with the hydroxyl hydrogens of these quenchers could then simply be another manifestation of the weak coupling limit of nonradiative decay. That is, the dioxorhenium/protic solvent complex possesses O–H stretching vibrations that could act as accepting modes in the nonradiative transition. No saturation of the quenching appears at high proton donor concentrations as would be expected from simple complex formation. Thus, unless the formation constant for the complex is exceptionally small, still more mechanisms must be contributing to the proton-enhanced decay of dioxorhenium excited states.

The $e \leftarrow b_2$ transition should be common to all d^1 and d^2 monooxo- and *trans*-dioxometal complexes. Species of this type are known for transition metals from groups 5–8, although luminescence only from dioxorhenium ions and molybdenyl ions[34] has been observed. There is ample reason to believe that many more metal–oxo complexes will possess long-lived $e \leftarrow b_2$ excited states that could participate in bimolecular photochemistry. Furthermore, our observation that protic solvents, especially water, efficiently quench the luminescence from dioxorhenium complexes suggests that the same could be true for many oxo species possessing different electronic structures. A search for luminescence from metal–oxo complexes dissolved in innocent (i.e., aprotic, unreactive) solvents could prove rewarding, especially in view of the fact that many such molecules luminesce in the solid state.[35] With the extra driving force derived from electronic excitation, metal–oxo photoredox chemistry should be a rich area for exploration.

Acknowledgment. J.R.W. thanks the Sun Co. for a graduate fellowship. This research was supported by National Science Foundation Grant CHE81-20419.

Registry No. $[ReO_2(en)_2]Cl$, 14405-69-7; $[ReO_2(py)_4]BPh_4$, 84417-09-4; $K_3ReO_2(CN)_4$, 19439-48-6; $[ReO_2(py\text{-}d_5)_4]BPh_4$, 84417-11-8; $[Re^{18}O_2(py)_4]BPh_4$, 84417-13-0; $[ReO_2(4\text{-pic})_4]BPh_4$, 84472-13-9; $[ReO_2(4\text{-}t\text{-Bupy})_4]BPh_4$, 84417-15-2.

Supplementary Material Available: Details of spin–orbit coupling calculations (4 pages). Ordering information is given on any current masthead page.

(32) Thomas, T. R.; Watts, R. J.; Crosby, G. A. *J. Chem. Phys.* **1973**, *59*, 2123–2131.
(33) Englman, R.; Jortner, J. *J. Mol. Phys.* **1970**, *18*, 145–164.
(34) Winkler, J. R.; Gray, H. B., to be submitted for publication.
(35) (a) Ronde, H.; Blasse, G. *J. Inorg. Nucl. Chem.* **1978**, *40*, 215–219. (b) Treadway, M. J.; Powell, P. C. *J. Chem. Phys.* **1974**, *61*, 4003–4011.